

# Prediction of dopant atoms distribution on nanocrystals using thermodynamic arguments

*Daniel G. Stroppa<sup>\*</sup>, Luciano A. Montoro, Antonio Campello, Lourdes Gracia, Armando Beltrán,  
Juan Andrés, Edson R. Leite, Antonio J. Ramirez*

## **Supporting Information contents:**

- Surface energy first principle calculations methodology
- HRTEM characterization of Sb:SnO<sub>2</sub> nanocrystals morphology

## **Corresponding Author**

\*d.stroppa@fz-juelich.de

Address: Ernst Ruska-Centre for Microscopy and Spectroscopy with Electrons (ER-C),  
Forschungszentrum Jülich GmbH, D-52425, Jülich, Germany.

Phone: +49 2461 61 2418; Fax: +49 2461 61 6444

## Surface energy first principle calculations methodology<sup>1</sup>

Surface energy calculations for Sb:SnO<sub>2</sub> nanocrystals were performed with the CRYSTAL06 program package.<sup>2</sup> Oxygen atoms were described by the standard 6-31G\* basis sets and the Tin and Antimony centres in the PS-21G\* scheme, where PS stands for Durand-Barthelet's non-relativistic large effective core potential.<sup>3</sup> Becke's three-parameter hybrid nonlocal exchange functional combined with the Lee-Yang-Parr gradient-corrected correlation functional (B3LYP) was used.<sup>4-5</sup> Full optimization of the cell parameters (a and c) and internal coordinate (u) for the bulk SnO<sub>2</sub> was carried out.

The low index (110), (101), (100) and (001) surfaces were modelled by stoichiometric unreconstructed (truncated bulk) slab models using the calculated equilibrium geometry. Because these surfaces have a different number of atoms in each layer, the low-index surfaces were modelled with different thicknesses in the z-direction but periodic in x- and y-directions. After the corresponding convergence test on the undoped systems, slab models containing nine SnO<sub>2</sub> layers for the (110), (100), and (101) surfaces and eleven layers for the (001) were selected. For the crystalline planes which may present more than one termination configuration, the choice was performed with basis on the higher structural stability and the lower total energy. O-terminated surfaces were considered for the {100}, {110} and {101} cases, as they were the most stable according to the calculation output. The {001} only present mixed Sn-O layers which are equivalent. A more extensive analysis regarding the surfaces termination in the SnO<sub>2</sub> same system is presented by Oviedo *et al.*<sup>6</sup> (Surface Science 463 (2000) 93–101).

A complete relaxation of all the atoms in each model was performed in order to evaluate the surface stress contribution on the surface energy value.

The surface energy value for the slab configurations were defined using the Equation S1, where the bulk cohesive energy per  $\text{SnO}_2$ , Sb or Sn unit formula is given by  $E_{bulk}$ , the slab total energy is given by  $E_{slab}$ , the supercell surface area is given by  $A$ , the number of  $\text{Sb}_x\text{Sn}_{1-x}\text{O}_2$  units is given by  $N$ , and the number of Sn atoms substituted by Sb is given by  $N.x$ .

$$E_{surf} = \lim_{N \rightarrow \infty} \left( E_{slab}^{N(\text{Sb}_x\text{Sn}_{1-x}\text{O}_2)} - N \left( E_{bulk}^{\text{SnO}_2} + x(E_{bulk}^{\text{Sb}} - E_{bulk}^{\text{Sn}}) \right) \right) / 2A \quad \text{Eq. S1}$$

Table S1 summarize the calculation results and important parameters used to build the atomic models. The slabs dimensions and actual compositions are indicated in for every calculation, as well as results for substitutions in sites with different symmetry (5f or 6f).

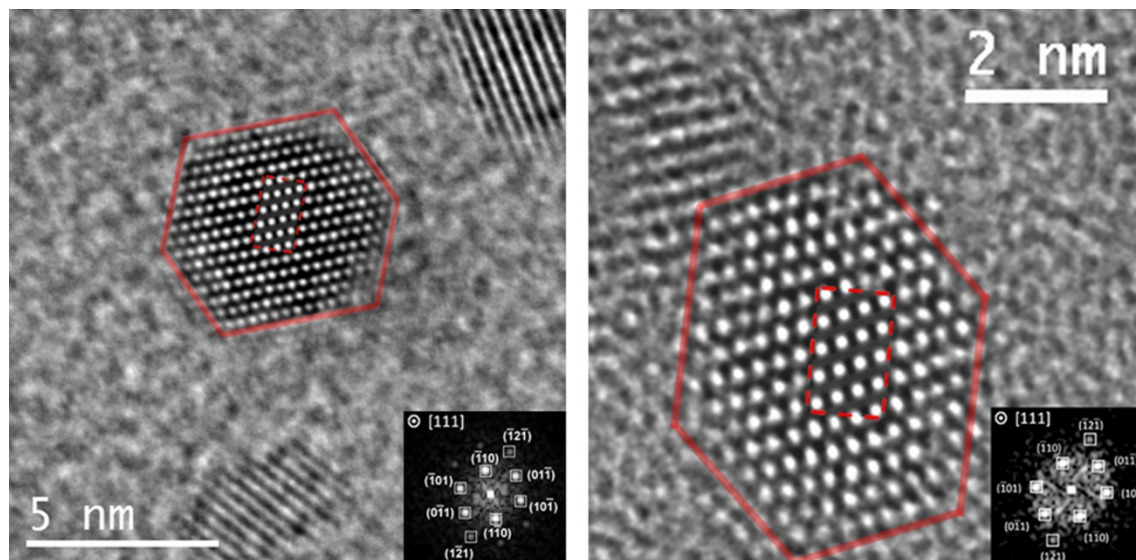
Surfaces	Sb dopant concentration (%at)			
	0	7.14	14.29	20
Surface energy ( $\text{J/m}^2$ ), cell atomic composition, slab area ( $\text{\AA}^2$ ) and width ( $\text{\AA}$ )				
(110)	2.04 $(\text{SnO}_2)_{14}$	4.20(5f) - 3.92(6f) $\text{Sn}_{26}\text{Sb}_2(\text{O}_2)_{28}$	6.33(5f) - 6.59(6f) $\text{Sn}_{12}\text{Sb}_2(\text{O}_2)_{14}$	6.31(6f) $\text{Sn}_8\text{Sb}_2(\text{O}_2)_{10}$
	21.15	42.31	21.15	21.15
	22.64	22.64	22.64	15.96
$(010) = (100)$	2.15 $(\text{SnO}_2)_7$	3.53 $\text{Sn}_{26}\text{Sb}_2(\text{O}_2)_{28}$	5.09 $\text{Sn}_{12}\text{Sb}_2(\text{O}_2)_{14}$	8.39 $\text{Sn}_8\text{Sb}_2(\text{O}_2)_{10}$
	14.96	59.83	29.92	14.96
	16.00	16.00	16.00	23.08
$(101) = (011)$	2.57 $(\text{SnO}_2)_{14}$	4.06 $\text{Sn}_{26}\text{Sb}_2(\text{O}_2)_{28}$	5.61 $\text{Sn}_{12}\text{Sb}_2(\text{O}_2)_{14}$	5.55 $\text{Sn}_8\text{Sb}_2(\text{O}_2)_{10}$
	26.87	53.75	26.87	26.87
	17.38	17.38	17.38	12.12
$(001)$	3.34 $(\text{SnO}_2)_{14}$	4.08 $\text{Sn}_{13}\text{Sb}(\text{O}_2)_{14}$	6.07 $\text{Sn}_{12}\text{Sb}_2(\text{O}_2)_{14}$	6.08 $\text{Sn}_8\text{Sb}_2(\text{O}_2)_{10}$
	22.33	22.33	22.33	22.33
	20.58	20.58	20.58	14.23

### HRTEM characterization of Sb:SnO<sub>2</sub> nanocrystals morphology

Sb:SnO<sub>2</sub> nanocrystals with two different Sb contents, 4.5%<sub>at</sub> and 13.9%<sub>at</sub> Sb doping concentration (measured composition), were synthesized in a glovebox under a controlled atmosphere by the benzyl alcohol method.<sup>7-8</sup> Stoichiometric amounts of SnCl<sub>4</sub> (99.995%) and SbCl<sub>3</sub> (99.99%) were stirred in a vessel with benzyl alcohol, after which the reaction vessel was removed from the glovebox and heated at 150°C for about 48h in a silicone bath. Sb:SnO<sub>2</sub> nanoparticles were collected by centrifugation, washed and stocked in tetrahydrofuran.

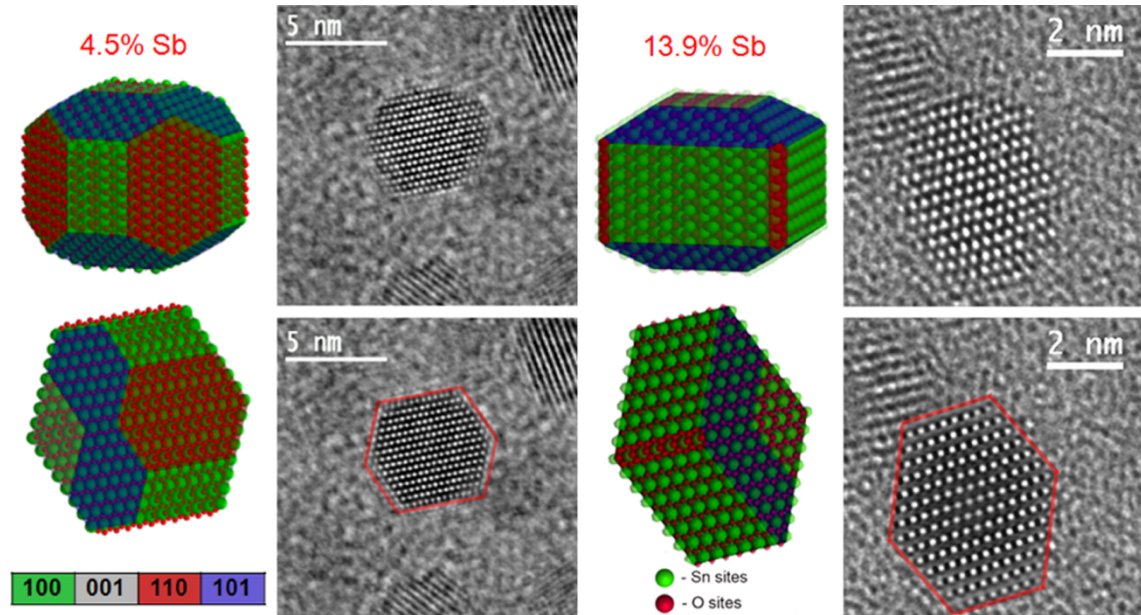
HRTEM characterization was performed using a JEM-2010 URP TEM at 200 kV with a LaB<sub>6</sub> electron gun and equipped with a 1024×1024 thermoelectrically cooled CCD camera and a XEDS detector. TEM samples were prepared by dripping diluted Sb:SnO<sub>2</sub> solution onto copper grids covered with a thin amorphous carbon film.

Figure S1 presents representative HRTEM images from the Sb:SnO<sub>2</sub> nanocrystals with 4.5%<sub>at</sub> and 13.9%<sub>at</sub> Sb doping contents, including the Fourier Transforms analysis and zone axes indexation, and the faceting outline.



**Figure S1.** HRTEM images and FFT indexation from a) 4.5%<sub>atom</sub> Sb-doped and b) 13.9%<sub>atom</sub> Sb-doped nanocrystals. The red continuous lines indicate the nanocrystals faceting and the dashed red lines indicate the results from multislice image simulation for the experimental imaging conditions. [From ref. [9], Copyright © 2011 by Wiley-VCH, reprinted with permission of authors.]

In order to describe the experimental nanocrystals geometry, nanocrystals models were constructed using the MEGACELL software<sup>10</sup> with basis on the number of projected atomic planes present on the experimental images and on the symmetry operations allowed by the SnO<sub>2</sub> unit cell. HRTEM simulated images of the nanocrystals models were obtained using JEMS software<sup>11</sup> and compared to the experimental images, as depicted on Figure S2. The nanocrystals models were refined by the qualitative comparison between simulated and experimental HRTEM images, and finally the nanocrystals dimensions were retrieved directly from the optimized nanocrystals models.



**Figure 2.** a) Trimetric and b) [111] zone axis oriented view for the 4.5%<sub>atom</sub> Sb-doped nanocrystals geometric model. c) Original HRTEM image from 4.5%<sub>atom</sub> Sb-doped nanocrystals and d) superimposition with the geometric model simulated HRTEM image. e) Trimetric and f) [111] zone axis oriented view for the 13.9%<sub>atom</sub> Sb-doped nanocrystals geometric model. g) Original HRTEM image from 13.9%<sub>atom</sub> Sb-doped nanocrystals and h) superimposition with the geometric model simulated HRTEM image. [From ref. [9], Copyright © 2011 by Wiley-VCH, reprinted with permission of authors.]

## References

- 1 - Beltrán, A.; Andrés, J.; Longo, E.; Leite, E. R.; *Appl. Phys. Lett.* **2003**, *83*, 635.
- 2 - Available at <http://www.crystal.unito.it/>.
- 3 - Durand, P.; Barthelat, J. C.; *Theoret. Chim. Acta* **1975**, *38* (4), 283-302.
- 4 - Becke, A. D.; *J. Chem. Phys.* **1993**, *98* (7), 5648-5652.
- 5 - Lee, C.; Yang, W.; Parr, R. G.; *Phys. Rev. B* **1988**, *37* (2), 785-789.
- 6 - Oviedo, J.; Gillan, M. J.; *Surface Science* **2000**, *463*, 93–101.
- 7 - Niederberger, M.; Gartwein, G.; *Chem. --Eur. J.* **2006**, *12* (28), 7282-7302.
- 8 - Da Silva, R. O.; Conti, T. G.; de Moura, A. F.; Stroppa, D. G.; Freitas, L. C. G.; Ribeiro, C.; Camargo, E. R.; Longo, E.; Leite, E. R.; *ChemPhysChem* **2009**, *10* (5), 841-846.
- 9 - Stroppa, D. G.; Montoro, L. A.; Beltrán, A.; Conti, T. G.; da Silva, R. O.; Andrés, J.; Leite, E. R.; Ramirez, A. J.; *Chem.--Eur. J.* **2011**, *17*, 11515-11519.
- 10 - Stroppa, D. G.; Righetto, R. D.; Montoro, L. A.; Ramirez, A. J.; *Ultramicroscopy* **2011**, *111*, 1077-1082.
- 11 - Stadelmann, P. A.; *Ultramicroscopy* **1987**, *21* (2), 131-145.